

Towards detection of relativistic effects in galaxy number counts using kSZ Tomography

Dagoberto Contreras^{1,2}, Matthew C. Johnson^{1,2}, and James B. Mertens^{1,2,3*}

¹*Department of Physics and Astronomy, York University, Toronto, Ontario, M3J 1P3, Canada*

²*Perimeter Institute for Theoretical Physics, Waterloo, Ontario N2L 2Y5, Canada and*

³*Canadian Institute for Theoretical Astrophysics,
University of Toronto, Toronto, ON M5H 3H8 Canada*

High-resolution, low-noise observations of the cosmic microwave background (CMB) planned for the near-future will enable new cosmological probes based on re-scattered CMB photons – the secondary CMB. At the same time, enormous galaxy surveys will map out huge volumes of the observable Universe. Using the technique of kinetic Sunyaev Zel'dovich (kSZ) tomography these new probes can be combined to reconstruct the remote dipole field, the CMB dipole as observed from different vantage points in our Universe. The volume accessible to future galaxy surveys is large enough that general relativistic corrections to the observed distribution of galaxies must be taken into account. These corrections are interesting probes of gravity in their own right, but can also obscure potential signatures of primordial non-Gaussianity. In this paper, we demonstrate that correlations between the reconstructed remote dipole field and the observed galaxy number counts can in principle be used to detect general relativistic corrections. We show that neglecting general relativistic corrections leads to an $\mathcal{O}(1)$ bias on the inferred amplitude of primordial non-Gaussianity, f_{NL} . In addition, we demonstrate that the reconstructed remote dipole field can provide useful constraining power on various bias parameters appearing in the galaxy number counts, and can significantly mitigate the effects of alignment bias.

I. INTRODUCTION

Galaxy surveys and cosmic microwave background (CMB) measurements will provide us with exceptionally accurate and precise measurements of our Universe over the coming decade. Galaxy surveys such as LSST [1] will produce massive redshift catalogues on the volume frontier, mapping out structures on ultra-large scales. Several exciting opportunities present themselves in the era of large-volume surveys, including the potential to measure subtle general relativistic effects in the observed clustering of galaxies [2–12] and an opportunity to detect primordial non-Gaussianity through its scale-dependent effect on galaxy bias [13]. CMB experiments such as Simons Observatory [14] and CMB-S4 [15] will produce measurements of the CMB on the sensitivity frontier, mapping out small-scale CMB temperature and polarization anisotropies near the nano-Kelvin level. At this sensitivity, it will be possible to accurately measure secondary CMB anisotropies such as the kinetic Sunyaev Zel'dovich (kSZ) effect [16], temperature anisotropies induced by the scattering of CMB photons from free electrons in bulk motion after reionization.

At first sight, these developments might appear only vaguely related. However, because the large scale structure (LSS) is responsible for the secondary CMB anisotropies, there is a strong correlation between the small-angular scale CMB and the distribution of structure probed by e.g. galaxy surveys. In the case of the kSZ effect, the statistical anisotropies in such correlations encode information about the structure of the Universe on the largest scales. This information can be extracted using a technique known as kSZ tomography [17–31], described in more detail below. In this paper, we demonstrate that a comparison of the large-scale distribution of galaxies to the large-scale inhomogeneities reconstructed using kSZ tomography can yield valuable new information about general relativistic contributions to the observed distribution of galaxies, with consequences for the measurement of primordial non-Gaussianity and various astrophysical bias parameters.

Considering the ways in which relativistic effects contribute to observables dates back to the birth of general relativity. In the present context, such effects arise from a precise treatment of photon geodesics in an inhomogeneous Universe. On large scales, cosmological perturbation theory is formulated within

*mertens@yorku.ca

general relativity (GR), so there are no additional “dynamical” effects to consider. The earliest perturbative calculations that carefully considered all relativistic contributions to observables for scalar perturbations are perhaps for fluctuations in the luminosity distance-redshift relation [2–5]. Considering these effects will be important for future supernova surveys to constrain the properties of dark energy [4]. Subsequently, the importance of relativistic effects has also been considered beyond leading order [6, 32–40], and in an exact, numerical setting [41, 42].

The galaxy number density as a function of redshift and angle on the sky—what we actually observe in a galaxy redshift survey—is also subject to relativistic corrections [7–12], similar in nature to effects commonly considered for other observables such as the CMB. In addition to the projected galaxy number density, redshift-space distortions (RSD; anisotropies in the mapping from real-space to redshift-space induced by peculiar velocities), magnification from lensing, and subdominant “general relativistic” (GR) effects also contribute to the observed number counts at linear order.¹ These GR effects include additional Doppler (magnification) terms and potential (Sachs-Wolfe, integrated Sachs-Wolfe, time delay) terms, analogous to the CMB. GR effects on number counts become important on scales approaching the cosmological horizon, and therefore are only accessible to surveys which have very large volume. Using a single tracer, it is unlikely that GR effects can be detected by any near-term survey [45, 46]. However, multi-tracer techniques can be used to pull them out [47]. Should these effects be detectable, they could serve as a probe of modifications to GR on ultra-large scales [48–50].

A prime science target of future galaxy surveys, for example LSST [1] and SPHEREX [51], is primordial non-Gaussianity (PNG); see [52] for an overview. Local-type PNG induces a scale-dependent galaxy bias [13], proportional to the parameter f_{NL} , leading to a measurable enhancement ($f_{NL} > 0$) or suppression ($f_{NL} < 0$) of galaxy clustering on the largest scales. An important milestone is constraining PNG at the level of $\sigma(f_{NL}) < 1$. This is because a generic prediction of a large class of multi-field inflationary models is $f_{NL} \sim \mathcal{O}(1)$, making a constraint at this level a potentially powerful discriminator between single-field and multi-field models of inflation [52, 53]. Both PNG and GR effects modify the galaxy-galaxy power spectrum on large physical/angular scales, making it important to incorporate both into forecasts for the constraining power of future experiments. In particular, it is known that neglecting GR effects can lead to an $\mathcal{O}(1)$ bias on measurements of f_{NL} [46]. A proper understanding of GR effects is therefore essential for properly interpreting future surveys, and the implication of their results for inflationary cosmology.

Measurements of PNG [54] and GR effects [47] can benefit greatly from incorporating cross-correlations of galaxy surveys with other tracers of the underlying dark matter distribution. In this case, a mode-by-mode comparison between the galaxy number density and dark matter density can be used to measure (scale-dependent) bias or to identify extra contributions to the observed galaxy number density from GR effects. Because such a comparison depends only on the properties of our observed realization, there is in principle no sample variance [54]. Taking advantage this “sample variance cancellation”, the ability to measure PNG or GR effects is limited only by the fidelity of the reconstruction of the dark matter density field (which depends on how correlated the tracer is with the distribution of dark matter) and shot noise on the galaxy survey.

Recently, kSZ tomography was introduced as a new and powerful tool for constraining PNG [30]. The kSZ effect induces CMB temperature anisotropies due to the scattering of CMB photons from free electrons in the post-reionization Universe. The kSZ effect comprises the dominant blackbody contribution to the observed CMB temperature on small angular scales ($\ell \gtrsim 4000$). A number of detections of the kSZ effect have been made with existing datasets [22, 55–62], and future experiments promise to obtain very high significance measurements [14, 15]. The amplitude of the kSZ temperature anisotropy from locations along our past light cone is proportional to the value of the remote dipole field, the projected temperature dipole at different locations in the observable Universe.

The three-dimensional remote dipole field can be reconstructed from statistical anisotropies in the cross-correlation between the CMB temperature on small angular scales and a galaxy survey, a technique called kSZ tomography [27–29]. The dominant contribution to the remote dipole field is the local peculiar velocity, which can be related to the dark matter density through linear theory. Correlating the reconstructed dipole field with the galaxy survey can therefore be used to isolate the scale-dependent galaxy bias due to PNG; the high fidelity of the reconstruction possible with future surveys allows one to take strong advantage of sample

¹ Rigorous treatments of relativistic effects have been extended to second order in [43, 44].

variance cancellation. Ref. [30] forecasted that it will in principle be possible to constrain PNG at the level of $\sigma(f_{\text{NL}}) < 1$ with the next generation of CMB instruments and galaxy surveys using kSZ tomography.

The present paper makes a number of important contributions to this previous analysis. First, we extend the analysis of Ref. [30], which utilized a simplified geometry, to the light cone. Our analysis includes all contributions to the remote dipole field beyond the local peculiar velocity (Doppler, Sachs-Wolfe, and integrated Sachs-Wolfe). We include RSD, lensing, and GR effects in the galaxy number density. We leave as free parameters in our model the redshift-dependent galaxy bias, evolution bias, magnification bias, and a multiplicative bias on the reconstructed remote dipole field that describes the optical depth degeneracy (see e.g. [63, 64]) in measurements of the kSZ effect (see Ref. [29] for an argument that this is sufficient). We also include an additional bias in the galaxy survey from intrinsic alignments due to large-scale tidal fields [65]. From here on we refer to such a bias as the alignment bias, defined explicitly in [65] and Appendix A. Finally, we include information from the primary CMB temperature and polarization in our constraints.

The goals of the present paper are to answer the questions:

- Is it possible to isolate GR effects in galaxy surveys using kSZ tomography?
- To what extent does neglecting GR effects bias the measurement of f_{NL} using kSZ tomography?
- Is sample variance cancellation between the remote dipole field and the galaxy survey useful for measuring various bias parameters?
- Does incorporating information from the primary CMB temperature and polarization help?

In summary, we find that kSZ tomography is a useful tool for isolating GR effects and improving the measurement of a variety of bias parameters when information from the primary CMB is incorporated. We further demonstrate that neglecting GR effects leads to an $\mathcal{O}(1)$ bias on measurements of f_{NL} from kSZ tomography.

The paper is structured as follows. In Sec. II, we outline the parameters of the Fisher forecast. In Sec. III, we discuss the results of our forecast, and in Sec. IV we conclude. A number of appendices are included to summarize the observables which go into our forecast.

II. FORECASTING METHOD

In order to address the questions posed in the introduction, we forecast the constraining power of future CMB measurements and galaxy surveys. Performing this forecast will require two main ingredients: one or more observable quantities, and any noise associated with measuring these observables. The observables we consider are angular power spectra,

$$C_{\ell}^{XY} = 4\pi \int \frac{dk}{k} \mathcal{P}(k) \Delta_{\ell}^X(k) \Delta_{\ell}^{Y*}(k), \quad (1)$$

where X and Y are one of: the perturbations in number counts of galaxies, the primary CMB temperature and polarization perturbations, or the remote dipole field reconstructed using kSZ tomography. Here, $\mathcal{P}(k)$ is the dimensionless primordial power spectrum,

$$\mathcal{P}(k) = A_s \left(\frac{k}{k_0} \right)^{n_s - 1}. \quad (2)$$

The noise associated with each of these observables will be shot noise in the case of galaxy number counts, instrument noise in the case of the primary CMB, and reconstruction noise in the case of the remote dipole field. The angular power spectra themselves are computed at linear order for the different tracers we consider. We explicitly state the form of the contributions to the transfer functions for number counts and the remote dipole field in Appendices A and B. The noise models we use are partly described below, and further details appear in these appendices, along with details on various bias functions that the transfer functions depend on.

As we are interested in exploring the importance of relativistic, non-Newtonian corrections, we parametrize the amplitude of these effects following [45]. We describe the amplitude of the relativistic corrections by

defining the parameters $\epsilon_{\text{GR}}^{\text{N}}$ and $\epsilon_{\text{GR}}^{\text{kSZ}}$, defined at the level of the transfer functions as

$$\Delta_{\ell}^{\text{N}}(k) = \Delta_{\ell}^{\text{D}}(k) + \Delta_{\ell}^{\text{RSD}}(k) + \Delta_{\ell}^{\text{L}}(k) + \epsilon_{\text{GR}}^{\text{N}} \Delta_{\ell}^{\text{N,GR}}(k) \quad (3)$$

$$\Delta_{\ell}^{\text{kSZ}}(k) = \Delta_{\ell}^{\text{LD}}(k) + \epsilon_{\text{GR}}^{\text{kSZ}} \Delta_{\ell}^{\text{kSZ,GR}}(k). \quad (4)$$

Here, the relativistic terms for number counts ($\Delta_{\ell}^{\text{N,GR}}$) include all effects except standard intrinsic density fluctuations (Δ_{ℓ}^{D}), RSD ($\Delta_{\ell}^{\text{RSD}}$), and lensing terms (Δ_{ℓ}^{L}), all of which are defined in Appendix A. While lensing itself is a general relativistic effect that must be taken into account, it has been considered separately in previous literature, and we follow this convention. The relativistic contributions to the remote dipole field ($\Delta_{\ell}^{\text{kSZ,GR}}$) we take to include all contributions except the local (Newtonian) peculiar velocity Doppler term ($\Delta_{\ell}^{\text{LD}}$). These contributions are also “primordial” in the sense that they represent the Sachs-Wolfe, Integrated Sachs-Wolfe, and primordial Doppler components.

We compute the galaxy number counts spectrum and reconstruct the remote dipole field in a set of redshift bins between $z \in [0.1, 3]$.² We divide this range into 30 bins equally spaced in comoving distance, and integrate the transfer functions over the redshift range within each bin weighted by tophat window functions (eg. $W_i(z)$ in Eq. A11 is a tophat). The width of these bins roughly corresponds to photometric redshift uncertainties, with $\sigma_z \sim 3/30 \sim 0.1$ in our binning scheme, although a more optimistic forecast could include additional bins as σ_z is projected to be of order 0.05 for an LSST-like survey, and as low as $\sigma_z \sim 0.02$ for a “red” galaxy population [1]. However, generally do not find that changing the number of bins strongly affects our constraints, as we illustrate further below.

Parameter	$\epsilon_{\text{GR}}^{\text{kSZ}}$	$\epsilon_{\text{GR}}^{\text{N}}$	f_{NL}	$10^{10} A_s$	n_s	Ω_b	Ω_c	h	τ	b_v^z	b_G^z	b_A^z	f_{evo}^z	s^z
Fiducial value	1	1	0	2.2	0.96	0.0528	0.2647	0.675	0.06	1	†	0	†	†

TABLE I: Cosmological and relativistic parameters, bias functions, and their fiducial values. The biases b_v , b_G , b_A , f_{evo} , s , that we refer to throughout are, respectively, the optical depth bias, the galaxy bias, the alignment bias, the evolution bias, and the magnification bias all defined explicitly in Appendix A and B. The values of bias functions indicated with a † vary with redshift, the modeling of which is described in Appendix A.

The final parameters we consider include standard cosmological ones, f_{NL} , bias parameters in each redshift bin, and the lightcone-projection/GR/primordial correction coefficients. In Table I we list each of the parameters we constrain, along with the fiducial values we use in our forecast.

We compute the Fisher matrix,

$$F_{\alpha\beta} = \sum_{\ell=1}^{\ell_{\text{max}}} \frac{2\ell+1}{2} \text{Tr} [(\partial_{\alpha} \mathcal{C}_{\ell}) \mathcal{C}_{\ell}^{-1} (\partial_{\beta} \mathcal{C}_{\ell}) \mathcal{C}_{\ell}^{-1}] + F_{\alpha\beta}^{\text{CMB, high-}\ell}, \quad (5)$$

for parameters α and β , and using a covariance matrix that includes all of the tracers,

$$\mathcal{C}_{\ell} = \begin{pmatrix} C_{\ell}^{\text{N,N}} & C_{\ell}^{\text{N,CMB}} & C_{\ell}^{\text{N,kSZ}} \\ C_{\ell}^{\text{CMB,N}} & C_{\ell}^{\text{CMB,CMB}} & C_{\ell}^{\text{CMB,kSZ}} \\ C_{\ell}^{\text{kSZ,N}} & C_{\ell}^{\text{kSZ,CMB}} & C_{\ell}^{\text{kSZ,kSZ}} \end{pmatrix} + N_{\ell}. \quad (6)$$

The C_{ℓ}^{XY} functions are the power spectra as defined in Eq. (1) and N_{ℓ} noise sources associated with these measurements, described in more detail below. These spectra are computed in each redshift bin for the remote dipole field and number counts; cross-spectra between all bins are accounted for, although this is not made explicit in Eq. (6). The CMB spectra are computed for both temperature and E -mode polarization. Derivatives are computed numerically with respect to the parameters $\{\Omega_b, \Omega_c, h, \tau\}$ using a second-order accurate upwind finite difference stencil. The remaining derivatives are computed analytically, explicitly commuting derivatives through any integrals over the redshift bins.

² kSZ tomography can in principle be performed at higher redshifts, however the number of observed galaxies beyond $z \sim 3$ in our fiducial survey is quite small, leading to a large reconstruction noise on the remote dipole field.

Due to the contributions from relativistic effects and non-Gaussianities manifesting on large scales, we consider auto- and cross-spectra of all tracers included in the forecast at low $\ell < 60$. We also account for the high- ℓ CMB temperature and E -mode constraints on cosmological parameters separately, using lensed CMB power spectra generated using CAMB. The Fisher matrix from this is included as the $F_{\alpha\beta}^{\text{CMB, high-}\ell}$ term in Eq. (5). In producing the high- ℓ CMB constraints, we have assumed a maximum available ℓ of 4000 in both T and E . The high- ℓ constraint is also only used to constrain the standard cosmological parameters $\{A_s, n_s, \Omega_b, \Omega_c, h, \tau\}$, and so elements are considered zero when an index corresponds to the remaining parameters and bias functions.

In order to study constraints from specific tracers or combinations of tracers, we can selectively exclude tracers from the covariance matrix C_ℓ by removing the row and column associated with a particular tracer, eg. removing the last column and row in order to neglect the contribution from the remote dipole field. When excluding the CMB, we also exclude the high- ℓ constraint (the $F_{\alpha\beta}^{\text{CMB, high-}\ell}$ term). In this way, we can examine how constraints from number counts alone improve as additional information is added from the primary CMB, and subsequently the remote dipole field.

The noise spectra N_ℓ are computed consistently for each observable we consider. For the primary CMB, we assume a CMB instrument noise of $1\mu\text{k-arcmin}$ for both temperature and polarization measurements (although we vary this later), and a 1 arcminute beam in each. Galaxy shot noise is computed from the luminosity function and limiting magnitude of the survey, as described in Appendix A. This is equivalent to the model adopted in Ref. [45]. The reconstruction noise for the remote dipole field is then computed following [28], using the galaxy number counts and CMB power spectra and noise described previously. We further assume that the electron distribution follows the dark matter distribution for our fiducial model. The uncertainty in this assumption is folded into the optical depth bias on the remote dipole, which we marginalize over in our analysis. For the reconstruction noise we assume a maximum available ℓ of $\ell_{\text{max}} = 9000$, which largely saturates the signal-to-noise of the relevant modes at the assumed CMB noise levels. We also assume that foregrounds and systematics can be mitigated and we do not consider these here. This may have an effect on the realistically accessible ℓ_{max} , and we comment on the implications for our constraints below.

We lastly seek to evaluate the bias in parameters, $\Delta\alpha$, due to neglecting various terms that arise from relativistic considerations. Following [46], we have

$$\Delta\alpha = (F^{-1})^{\alpha\beta} v_\beta, \quad (7)$$

where F^{-1} is the inverse fisher matrix, and

$$v_\beta = \sum_{\ell=1}^{\ell_{\text{max}}} \frac{2\ell+1}{2} \text{Tr} [(\partial_\alpha C_\ell) C_\ell^{-1} \Delta C_\ell C_\ell^{-1}], \quad (8)$$

where $\Delta C_\ell = C_\ell^{\text{true}} - C_\ell^{\text{fiducial}}$. The quantity $\Delta\alpha$ then describes the extent to which the measurement of a parameter α is biased when assuming a fiducial spectrum C_ℓ^{fiducial} instead of using the true spectrum C_ℓ^{true} . The fiducial spectrum we use here is the one where the general relativistic contributions are neglected in both the number counts and kSZ measurements, ie. the transfer functions are evaluated with $\epsilon_{\text{GR}}^{\text{kSZ}} = 0$ and $\epsilon_{\text{GR}}^N = 0$.

III. RESULTS

We now examine the impact of the relativistic effects on future observations of galaxy number counts, CMB temperature and polarization, and the reconstruction of the remote dipole field. We wish to highlight the importance of alignment bias in the context of number counts alone. We explicitly focus on this as alignment bias is often not taken into account in forecasts, yet has the potential to interfere with measurements of the growth function and galaxy bias, thereby degrading constraints on cosmological parameters. We then incorporate both primary CMB measurements, and the remote dipole field into the forecast, and explore how constraints change as each new observable is included. We will demonstrate that the degradation on parameter constraints incurred by including the alignment bias is no longer an issue once CMB and kSZ tomography are included. In particular constraints on f_{evo} are dramatically improved when kSZ tomography is used (for $z \lesssim 2.5$).

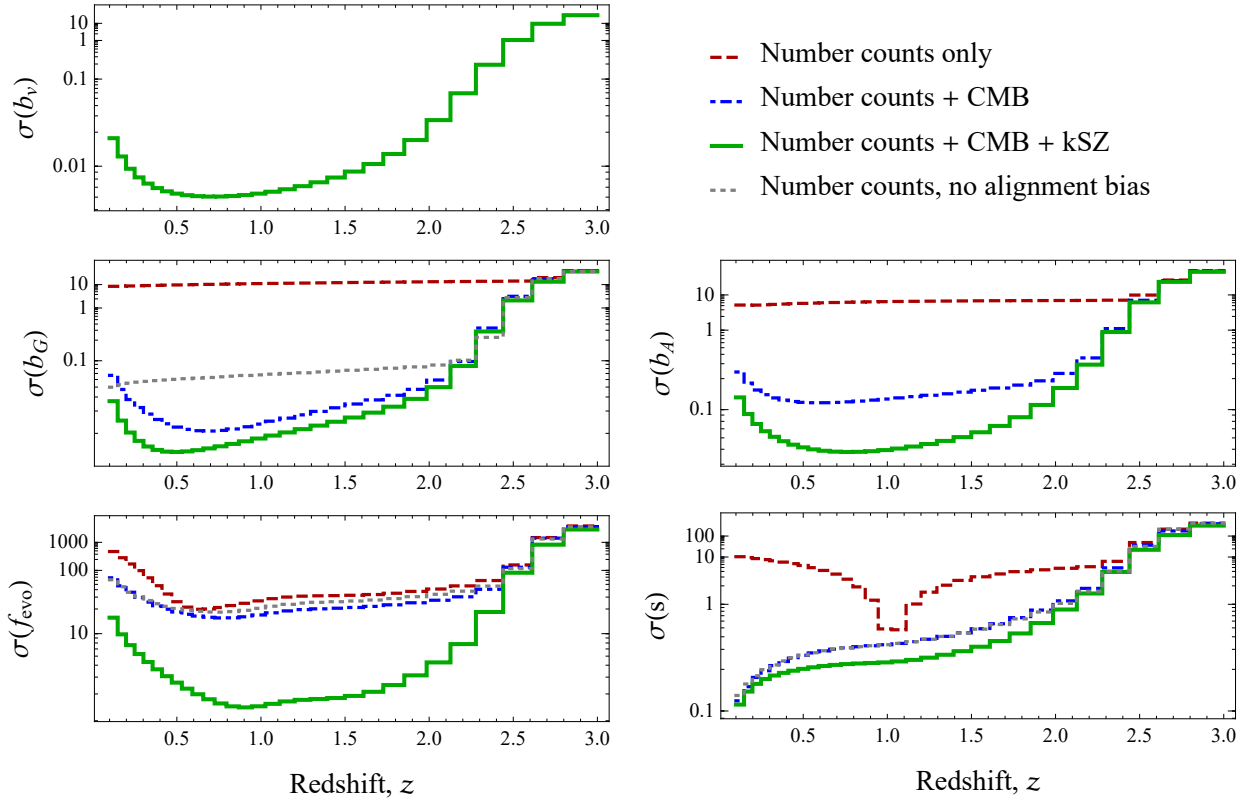


FIG. 1: Constraints on various biases as a function of redshift bin, including different combinations of tracers as indicated by the legend. Constraints without accounting for alignment bias are also shown. “Steps” indicate the width of the redshift bins.

	N	N, no \$b_A\$	N + CMB	N + CMB + kSZ	N + CMB + kSZ + \$f_{\text{evo}}\$ prior
$\sigma(f_{\text{NL}})$	16	14	9.0	1.3	1.0
$b(f_{\text{NL}})$	-9.3	-8.3	-2.2	-2.0	-3.3
$\sigma(\epsilon_{\text{GR}}^N)$	5.1	4.1	3.2	0.58	0.09
$\sigma(\epsilon_{\text{GR}}^{\text{kSZ}})$	—	—	—	0.61	0.60

TABLE II: Forecasted uncertainties on parameters of interest, and bias on f_{NL} due to neglecting relativistic effects from number counts and kSZ measurements. Forecasts are shown with and without alignment bias, and as additional observables and priors are added.

We begin by examining constraints on the various bias functions in Fig. 1. These can be seen to drastically deteriorate as alignment bias is taken into account (compare the gray-dashed curves with the others), especially galaxy bias with which the alignment bias is degenerate. The bias functions subsequently recover as information from the CMB is included in the constraint. Notably, beyond the primary CMB and number counts alone, kSZ tomography can offer a substantial improvement in constraints on these biases, from a factor of a few, up to an order of magnitude in the case of evolution bias (for $z \lesssim 2.5$). No priors on any parameters are included in the constraints in this figure, and cosmological parameters including f_{NL} and the ϵ_{GR} parameters are marginalized over.

The fiducial values of the galaxy and magnification bias as described in Appendix A are of order unity,

and thus should be detected at high significance. The evolution bias is somewhat smaller, so detection prospects are perhaps marginal even when including information from kSZ tomography in the constraint. The evolution bias itself is degenerate with the amplitude of relativistic effects, and to a smaller extent f_{NL} . An improved constraint on this bias can therefore help to reduce forecasted uncertainties, especially in ϵ_{GR}^N . The amplitude of the alignment bias, on the other hand, is expected to be at most a few percent [65]; while also marginal, we find that kSZ tomography may offer a way to detect alignment bias. The bias due to optical depth degeneracy, b_v , is only constrained when including information from the remote dipole field. The sub-percent constraint on b_v is highly significant relative to the fiducial value of unity of this bias, and is comparable to constraints forecasted using other methods [66].

We next examine how detectable relativistic contributions to observables are, looking at ϵ_{GR}^N and $\epsilon_{\text{GR}}^{\text{kSZ}}$, along with how an inferred bias for f_{NL} may be incurred when neglecting relativistic effects. The constraints and bias values are listed in Table II. These have been marginalized over other cosmological parameters noted in Table (I), as well as all bias functions, including the bias due to the kSZ optical depth degeneracy where relevant. In both the case where we include and neglect alignment bias, relativistic effects are not detectable with number counts alone, and the bias due to neglecting these effects is unimportant. As constraints from the primary CMB are added, which primarily serve to pin down standard cosmological parameters, constraints on relativistic effects recover from alignment bias. As the reconstructed kSZ remote dipole field is included in the analysis, the constraints improve substantially, to the point where both a bias on f_{NL} and relativistic effects are detectable at moderate significance.

Following [45], we also consider the impact of including a Gaussian prior on the evolution bias of $\Delta f_{\text{evo}} = 1$ in all redshift bins. The constraints on relativistic effects we find are then comparable to the multiple tracers considered in [47], however the prior we use is significantly less strict. We additionally consider what happens when we do not simultaneously constrain the ϵ_{GR} parameters and f_{NL} : this improves constraints to $\sigma(f_{\text{NL}}) \sim 0.9$ both with and without the evolution bias prior.

Using all tracers considered—number counts including alignment bias and the f_{evo} prior, the primary CMB, and the remote dipole field—we lastly explore the constraints as a function of instrumental parameters. We show these in Figure 2, as the CMB experiment noise, number of redshift bins (ie. photometric redshift error), and limiting magnitude are varied about the fiducial values considered above. The constraints presented in these figures include the evolution bias prior.

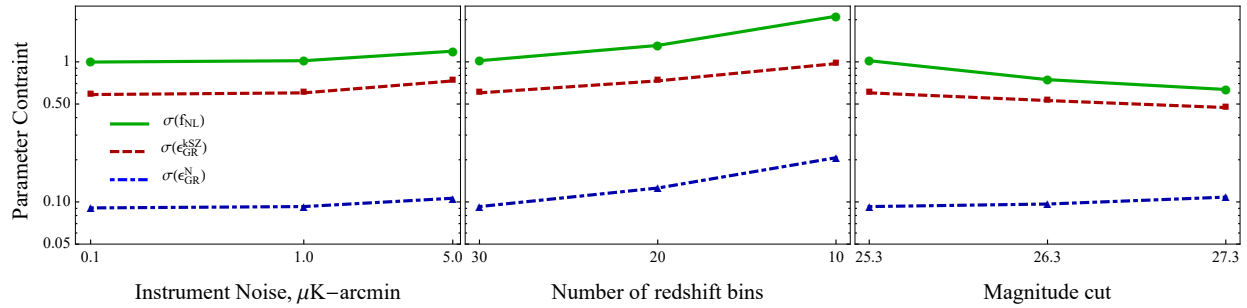


FIG. 2: Forecasted uncertainty in parameters as experimental parameters are varied. Fiducial parameters include 1 $\mu\text{K-arcmin}$ noise, 30 bins, and a magnitude limit of $r = 25.3$ (magnitude limit discussed in more detail in Appendix A).

Generally, the constraints improve as one might expect. Increasing CMB instrument noise results in higher reconstruction noise on the remote dipole field, and constraints on the parameters we consider all become mildly worse. Decreasing the number of redshift bins (e.g. increasing the photometric redshift error) similarly reduces the information available, resulting again in moderately worse constraints. Varying the limiting magnitude of the galaxy survey provides a more complicated picture: constraints on f_{NL} and $\epsilon_{\text{GR}}^{\text{kSZ}}$ improve, while constraints on ϵ_{GR}^N actually worsen. This is because the fiducial bias model changes in such a way that the signal of relativistic effects (as well as lensing, which we do not consider) all decrease relative to intrinsic density perturbations and RSD effects. The “noise” due to cosmic variance from these dominant effects is therefore increased, resulting in a worse overall constraint on relativistic effects.

IV. CONCLUSIONS AND DISCUSSION

In this paper, we have illustrated the potential importance of the remote dipole field reconstructed using kSZ tomography for the detectability of relativistic effects in galaxy number counts, and the need to account for relativistic effects to obtain an unbiased measurement of primordial non-Gaussianity using kSZ tomography. We also highlighted the improvement on the measurement of various (redshift-dependent) bias parameters from the correlation between the remote dipole field and number counts. The forecasted constraints on most bias parameters can improve by a factor of a few, and constraints on the evolution bias can improve by more than an order of magnitude. This is significant, as evolution bias is strongly degenerate with both relativistic effects and scale-dependent bias from primordial non-Gaussianity. Even with this improvement, evolution bias is poorly constrained; we demonstrate that a weak prior can substantially improve the detectability of relativistic effects. Importantly, our analysis shows that kSZ tomography can significantly mitigate the effects of alignment bias, which can seriously degrade constraints on primordial non-Gaussianity using number counts alone.

Our forecasts have included a number of optimistic assumptions. In particular, we have presented the constraints in the limit where we have data on the full sky and foregrounds and systematics are negligible. Partial-sky data will weaken measurements on the largest scales, which could significantly degrade constraints on relativistic effects and primordial non-Gaussianity. Foregrounds and systematics on small angular scales have the potential to degrade the reconstruction of the remote dipole field. To estimate the effect this might have, we repeated our forecast using an ℓ_{\max} of 5000 in the reconstruction noise. This yields only a roughly 25 % increase in our forecasted uncertainties.

Several additional assumptions made in this work are perhaps pessimistic. For example, the galaxy number counts we compute contain very few observable galaxies beyond redshift $z \sim 2$, while calculations of the galaxy number counts using different assumptions can yield a higher number of galaxies at comparable redshifts (see e.g. [29, 67] for similar studies). The magnitude limits we assume are also conservative, and information from fainter galaxies up to a magnitude of $r \sim 27.5$ may be accessible, albeit with larger uncertainties in photometric redshifts. We have also not split our analysis into separate galaxy populations (red, blue) nor included additional tracers, such as intensity mapping, that have been shown to improve constraints [45–47].

While changing our assumptions about the fiducial CMB and galaxy surveys has the potential to nudge our forecasted uncertainties up or down, this work demonstrates that kSZ tomography promises to be an important and useful tool for isolating both relativistic effects and new physics. We have further highlighted a significant bias on measurements of primordial non-Gaussianity incurred when relativistic effects are neglected, and illustrated a significant improvement on various bias functions that can be obtained using kSZ tomography. This paper strengthens the science case for performing kSZ tomography using future observations.

V. ACKNOWLEDGMENTS

We would like to thank Juan Cayuso, Neal Dalal, and Moritz Munchmeyer for helpful discussions. This research was enabled in part by support provided by the Shared Hierarchical Academic Research Computing Network (SHARCNET:www.sharcnet.ca), Compute Canada (www.computecanada.ca), and the Kenyon College Department of Physics. This research was supported in part by Perimeter Institute for Theoretical Physics. Research at Perimeter Institute is supported by the Government of Canada through the Department of Innovation, Science and Economic Development Canada and by the Province of Ontario through the Ministry of Research, Innovation and Science. MCJ and DC were supported by the National Science and Engineering Research Council through a Discovery grant. JBM acknowledges support as a CITA National Fellow.

[1] **LSST Science, LSST Project** Collaboration, P. A. Abell *et al.*, “LSST Science Book, Version 2.0,” arXiv:0912.0201 [astro-ph.IM].

- [2] M. Sasaki, “The Magnitude - Redshift relation in a perturbed Friedmann universe,” *Mon. Not. Roy. Astron. Soc.* **228** (1987) 653–669.
- [3] T. Pyne and M. Birkinshaw, “The luminosity distance in perturbed flrw spacetimes,” *Mon. Not. Roy. Astron. Soc.* **348** (2004) 581, [arXiv:astro-ph/0310841](https://arxiv.org/abs/astro-ph/0310841) [astro-ph].
- [4] L. Hui and P. B. Greene, “Correlated Fluctuations in Luminosity Distance and the (Surprising) Importance of Peculiar Motion in Supernova Surveys,” *Phys. Rev. D* **73** (2006) 123526, [arXiv:astro-ph/0512159](https://arxiv.org/abs/astro-ph/0512159) [astro-ph].
- [5] C. Bonvin, R. Durrer, and M. A. Gasparini, “Fluctuations of the luminosity distance,” *Phys. Rev. D* **73** (2006) 023523, [arXiv:astro-ph/0511183](https://arxiv.org/abs/astro-ph/0511183) [astro-ph]. [Erratum: Phys. Rev.D85,029901(2012)].
- [6] E. Barausse, S. Matarrese, and A. Riotto, “The Effect of inhomogeneities on the luminosity distance-redshift relation: Is dark energy necessary in a perturbed Universe?,” *Phys. Rev. D* **71** (2005) 063537, [arXiv:astro-ph/0501152](https://arxiv.org/abs/astro-ph/0501152) [astro-ph].
- [7] J. Yoo, “Complete Treatment of Galaxy Two-Point Statistics: Gravitational Lensing Effects and Redshift-Space Distortions,” *Phys. Rev. D* **79** (2009) 023517, [arXiv:0808.3138](https://arxiv.org/abs/0808.3138) [astro-ph].
- [8] J. Yoo, A. L. Fitzpatrick, and M. Zaldarriaga, “New perspective on galaxy clustering as a cosmological probe: General relativistic effects,” *Phys. Rev. D* **80** (Oct, 2009) 083514, [arXiv:0907.0707](https://arxiv.org/abs/0907.0707) [astro-ph.CO].
- [9] J. Yoo, “General Relativistic Description of the Observed Galaxy Power Spectrum: Do We Understand What We Measure?,” *Phys. Rev. D* **82** (2010) 083508, [arXiv:1009.3021](https://arxiv.org/abs/1009.3021) [astro-ph.CO].
- [10] C. Bonvin and R. Durrer, “What galaxy surveys really measure,” *Phys. Rev. D* **84** (2011) 063505, [arXiv:1105.5280](https://arxiv.org/abs/1105.5280) [astro-ph.CO].
- [11] A. Challinor and A. Lewis, “The linear power spectrum of observed source number counts,” *Phys. Rev. D* **84** (2011) 043516, [arXiv:1105.5292](https://arxiv.org/abs/1105.5292) [astro-ph.CO].
- [12] D. Jeong, F. Schmidt, and C. M. Hirata, “Large-scale clustering of galaxies in general relativity,” *Phys. Rev. D* **85** (2012) 023504, [arXiv:1107.5427](https://arxiv.org/abs/1107.5427) [astro-ph.CO].
- [13] N. Dalal, O. Dore, D. Huterer, and A. Shirokov, “The imprints of primordial non-gaussianities on large-scale structure: scale dependent bias and abundance of virialized objects,” *Phys. Rev. D* **77** (2008) 123514, [arXiv:0710.4560](https://arxiv.org/abs/0710.4560) [astro-ph].
- [14] **Simons Observatory** Collaboration, J. Aguirre *et al.*, “The Simons Observatory: Science goals and forecasts,” *JCAP* **1902** (2019) 056, [arXiv:1808.07445](https://arxiv.org/abs/1808.07445) [astro-ph.CO].
- [15] **CMB-S4** Collaboration, K. N. Abazajian *et al.*, “CMB-S4 Science Book, First Edition,” [arXiv:1610.02743](https://arxiv.org/abs/1610.02743) [astro-ph.CO].
- [16] R. A. Sunyaev and I. B. Zeldovich, “The velocity of clusters of galaxies relative to the microwave background - The possibility of its measurement,” *MNRAS* **190** (Feb., 1980) 413–420.
- [17] S. Ho, S. Dedeo, and D. Spergel, “Finding the Missing Baryons Using CMB as a Backlight,” *ArXiv e-prints* (Mar., 2009) , [arXiv:0903.2845](https://arxiv.org/abs/0903.2845) [astro-ph.CO].
- [18] J. Shao, P. Zhang, W. Lin, Y. Jing, and J. Pan, “Kinetic Sunyaev-Zel’dovich tomography with spectroscopic redshift surveys,” *MNRAS* **413** (May, 2011) 628–642, [arXiv:1004.1301](https://arxiv.org/abs/1004.1301) [astro-ph.CO].
- [19] P. Zhang and A. Stebbins, “Confirmation of the Copernican Principle at Gpc Radial Scale and above from the Kinetic Sunyaev-Zel’dovich Effect Power Spectrum,” *Physical Review Letters* **107** no. 4, (July, 2011) 041301.
- [20] P. Zhang and U.-L. Pen, “Deprojecting Sunyaev-Zeldovich Statistics,” *Astrophys. J.* **549** (Mar., 2001) 18–27, [astro-ph/0007462](https://arxiv.org/abs/astro-ph/0007462).
- [21] D. Munshi, I. T. Iliev, K. L. Dixon, and P. Coles, “Extracting the late-time kinetic Sunyaev-Zel’dovich effect,” [arXiv:1511.03449](https://arxiv.org/abs/1511.03449) [astro-ph.CO].
- [22] **ACTPol** Collaboration, E. Schaan *et al.*, “Evidence for the kinematic Sunyaev-Zel’dovich effect with the Atacama Cosmology Telescope and velocity reconstruction from the Baryon Oscillation Spectroscopic Survey,” *Phys. Rev. D* **93** no. 8, (2016) 082002, [arXiv:1510.06442](https://arxiv.org/abs/1510.06442) [astro-ph.CO].
- [23] S. Ferraro, J. C. Hill, N. Battaglia, J. Liu, and D. N. Spergel, “The Kinematic Sunyaev-Zel’dovich Effect with Projected Fields II: prospects, challenges, and comparison with simulations,” [arXiv:1605.02722](https://arxiv.org/abs/1605.02722) [astro-ph.CO].
- [24] J. C. Hill, S. Ferraro, N. Battaglia, J. Liu, and D. N. Spergel, “Kinematic Sunyaev-Zel’dovich Effect with Projected Fields: A Novel Probe of the Baryon Distribution with Planck, WMAP, and WISE Data,” *Phys. Rev. Lett.* **117** no. 5, (2016) 051301, [arXiv:1603.01608](https://arxiv.org/abs/1603.01608) [astro-ph.CO].
- [25] P. Zhang, “The dark flow induced small-scale kinetic Sunyaev-Zel’dovich effect,” *MNRAS* **407** (Sept., 2010) L36–L40, [arXiv:1004.0990](https://arxiv.org/abs/1004.0990) [astro-ph.CO].
- [26] P. Zhang and M. C. Johnson, “Testing eternal inflation with the kinetic Sunyaev Zel’dovich effect,” *JCAP* **1506** no. 06, (2015) 046, [arXiv:1501.00511](https://arxiv.org/abs/1501.00511) [astro-ph.CO].
- [27] A. Terrana, M.-J. Harris, and M. C. Johnson, “Analyzing the cosmic variance limit of remote dipole measurements of the cosmic microwave background using the large-scale kinetic Sunyaev Zel’dovich effect,” *Journal of Cosmology and Astroparticle Physics* **2017** no. 02, (Feb, 2017) 040–040, [arXiv:1610.06919](https://arxiv.org/abs/1610.06919).
- [28] A.-S. Deutsch, E. Dimastrogiovanni, M. C. Johnson, M. Münchmeyer, and A. Terrana, “Reconstruction of the remote dipole and quadrupole fields from the kinetic Sunyaev Zel’dovich and polarized Sunyaev Zel’dovich effects,” *Phys. Rev. D* **98** no. 12, (2018) 123501, [arXiv:1707.08129](https://arxiv.org/abs/1707.08129) [astro-ph.CO].

[29] K. M. Smith, M. S. Madhavacheril, M. Münchmeyer, S. Ferraro, U. Giri, and M. C. Johnson, “KSZ tomography and the bispectrum,” [arXiv:1810.13423](https://arxiv.org/abs/1810.13423) [astro-ph.CO].

[30] M. Münchmeyer, M. S. Madhavacheril, S. Ferraro, M. C. Johnson, and K. M. Smith, “Constraining local non-Gaussianities with kSZ tomography,” [arXiv:1810.13424](https://arxiv.org/abs/1810.13424) [astro-ph.CO].

[31] N. Sehgal *et al.*, “Science from an Ultra-Deep, High-Resolution Millimeter-Wave Survey,” [arXiv:1903.03263](https://arxiv.org/abs/1903.03263) [astro-ph.CO].

[32] D. Bertacca, R. Maartens, A. Raccanelli, and C. Clarkson, “Beyond the plane-parallel and Newtonian approach: Wide-angle redshift distortions and convergence in general relativity,” *JCAP* **1210** (2012) 025, [arXiv:1205.5221](https://arxiv.org/abs/1205.5221) [astro-ph.CO].

[33] I. Ben-Dayan, M. Gasperini, G. Marozzi, F. Nugier, and G. Veneziano, “Do stochastic inhomogeneities affect dark-energy precision measurements?,” *Phys. Rev. Lett.* **110** no. 2, (2013) 021301, [arXiv:1207.1286](https://arxiv.org/abs/1207.1286) [astro-ph.CO].

[34] O. Umeh, C. Clarkson, and R. Maartens, “Nonlinear relativistic corrections to cosmological distances, redshift and gravitational lensing magnification: I. Key results,” *Class. Quant. Grav.* **31** (2014) 202001, [arXiv:1207.2109](https://arxiv.org/abs/1207.2109) [astro-ph.CO].

[35] I. Ben-Dayan, R. Durrer, G. Marozzi, and D. J. Schwarz, “The value of H_0 in the inhomogeneous Universe,” *Phys. Rev. Lett.* **112** (2014) 221301, [arXiv:1401.7973](https://arxiv.org/abs/1401.7973) [astro-ph.CO].

[36] O. Umeh, C. Clarkson, and R. Maartens, “Nonlinear relativistic corrections to cosmological distances, redshift and gravitational lensing magnification. II - Derivation,” *Class. Quant. Grav.* **31** (2014) 205001, [arXiv:1402.1933](https://arxiv.org/abs/1402.1933) [astro-ph.CO].

[37] C. Clarkson, O. Umeh, R. Maartens, and R. Durrer, “What is the distance to the CMB?,” *JCAP* **1411** no. 11, (2014) 036, [arXiv:1405.7860](https://arxiv.org/abs/1405.7860) [astro-ph.CO].

[38] G. Marozzi, “The luminosity distance-redshift relation up to second order in the Poisson gauge with anisotropic stress,” *Class. Quant. Grav.* **32** no. 4, (2015) 045004, [arXiv:1406.1135](https://arxiv.org/abs/1406.1135) [astro-ph.CO]. [erratum: *Class. Quant. Grav.* **32**, 179501 (2015)].

[39] J. Yoo and M. Zaldarriaga, “Beyond the Linear-Order Relativistic Effect in Galaxy Clustering: Second-Order Gauge-Invariant Formalism,” *Phys. Rev.* **D90** no. 2, (2014) 023513, [arXiv:1406.4140](https://arxiv.org/abs/1406.4140) [astro-ph.CO].

[40] J. Adamek, C. Clarkson, L. Coates, R. Durrer, and M. Kunz, “Bias and scatter in the Hubble diagram from cosmological large-scale structure,” [arXiv:1812.04336](https://arxiv.org/abs/1812.04336) [astro-ph.CO].

[41] J. T. Giblin, J. B. Mertens, and G. D. Starkman, “Observable Deviations from Homogeneity in an Inhomogeneous Universe,” *Astrophys. J.* **833** no. 2, (2016) 247, [arXiv:1608.04403](https://arxiv.org/abs/1608.04403) [astro-ph.CO].

[42] J. T. Giblin, J. B. Mertens, G. D. Starkman, and A. R. Zentner, “General Relativistic Corrections to the Weak Lensing Convergence Power Spectrum,” *Phys. Rev.* **D96** no. 10, (2017) 103530, [arXiv:1707.06640](https://arxiv.org/abs/1707.06640) [astro-ph.CO].

[43] D. Bertacca, R. Maartens, and C. Clarkson, “Observed galaxy number counts on the lightcone up to second order: I. Main result,” *JCAP* **1409** no. 09, (2014) 037, [arXiv:1405.4403](https://arxiv.org/abs/1405.4403) [astro-ph.CO].

[44] D. Bertacca, R. Maartens, and C. Clarkson, “Observed galaxy number counts on the lightcone up to second order: II. Derivation,” *JCAP* **1411** no. 11, (2014) 013, [arXiv:1406.0319](https://arxiv.org/abs/1406.0319) [astro-ph.CO].

[45] D. Alonso, P. Bull, P. G. Ferreira, R. Maartens, and M. Santos, “Ultra large-scale cosmology in next-generation experiments with single tracers,” *Astrophys. J.* **814** no. 2, (2015) 145, [arXiv:1505.07596](https://arxiv.org/abs/1505.07596) [astro-ph.CO].

[46] C. S. Lorenz, D. Alonso, and P. G. Ferreira, “Impact of relativistic effects on cosmological parameter estimation,” *Phys. Rev.* **D97** no. 2, (2018) 023537, [arXiv:1710.02477](https://arxiv.org/abs/1710.02477) [astro-ph.CO].

[47] D. Alonso and P. G. Ferreira, “Constraining ultralarge-scale cosmology with multiple tracers in optical and radio surveys,” *Phys. Rev.* **D92** no. 6, (2015) 063525, [arXiv:1507.03550](https://arxiv.org/abs/1507.03550) [astro-ph.CO].

[48] T. Baker and P. Bull, “Observational signatures of modified gravity on ultra-large scales,” *Astrophys. J.* **811** (2015) 116, [arXiv:1506.00641](https://arxiv.org/abs/1506.00641) [astro-ph.CO].

[49] J. Renk, M. Zumalacarregui, and F. Montanari, “Gravity at the horizon: on relativistic effects, CMB-LSS correlations and ultra-large scales in Horndeski’s theory,” *JCAP* **1607** no. 07, (2016) 040, [arXiv:1604.03487](https://arxiv.org/abs/1604.03487) [astro-ph.CO].

[50] D. Duniya, T. Moloi, C. Clarkson, J. Larena, R. Maartens, B. Mongwane, and A. Weltman, “Probing beyond-Horndeski gravity on ultra-large scales,” [arXiv:1902.09919](https://arxiv.org/abs/1902.09919) [astro-ph.CO].

[51] O. Doré *et al.*, “Cosmology with the SPHEREX All-Sky Spectral Survey,” [arXiv:1412.4872](https://arxiv.org/abs/1412.4872) [astro-ph.CO].

[52] M. Alvarez *et al.*, “Testing Inflation with Large Scale Structure: Connecting Hopes with Reality,” [arXiv:1412.4671](https://arxiv.org/abs/1412.4671) [astro-ph.CO].

[53] N. Bartolo, E. Komatsu, S. Matarrese, and A. Riotto, “Non-Gaussianity from inflation: Theory and observations,” *Phys. Rept.* **402** (2004) 103–266, [arXiv:astro-ph/0406398](https://arxiv.org/abs/astro-ph/0406398) [astro-ph].

[54] U. Seljak, “Extracting primordial non-gaussianity without cosmic variance,” *Phys. Rev. Lett.* **102** (2009) 021302, [arXiv:0807.1770](https://arxiv.org/abs/0807.1770) [astro-ph].

[55] N. Hand *et al.*, “Evidence of Galaxy Cluster Motions with the Kinematic Sunyaev-Zel’dovich Effect,” *Phys. Rev. Lett.* **109** (2012) 041101, [arXiv:1203.4219](https://arxiv.org/abs/1203.4219) [astro-ph.CO].

[56] **Planck** Collaboration, “Planck intermediate results. XXXVII. Evidence of unbound gas from the kinetic

Sunyaev-Zeldovich effect,” *Astron. Astrophys.* **586** (2016) A140, [arXiv:1504.03339 \[astro-ph.CO\]](https://arxiv.org/abs/1504.03339).

[57] F. De Bernardis *et al.*, “Detection of the pairwise kinematic Sunyaev-Zel’dovich effect with BOSS DR11 and the Atacama Cosmology Telescope,” *JCAP* **1703** no. 03, (2017) 008, [arXiv:1607.02139 \[astro-ph.CO\]](https://arxiv.org/abs/1607.02139).

[58] **DES, SPT** Collaboration, B. Soergel *et al.*, “Detection of the kinematic Sunyaev-Zel’dovich effect with DES Year 1 and SPT,” *Mon. Not. Roy. Astron. Soc.* **461** no. 3, (2016) 3172–3193, [arXiv:1603.03904 \[astro-ph.CO\]](https://arxiv.org/abs/1603.03904).

[59] N. S. Sugiyama, T. Okumura, and D. N. Spergel, “A direct measure of free electron gas via the kinematic Sunyaev-Zel’dovich effect in Fourier-space analysis,” *Mon. Not. Roy. Astron. Soc.* **475** no. 3, (2018) 3764–3785, [arXiv:1705.07449 \[astro-ph.CO\]](https://arxiv.org/abs/1705.07449).

[60] Y.-C. Li, Y.-Z. Ma, M. Remazeilles, and K. Moodley, “Measurement of the pairwise kinematic Sunyaev-Zeldovich effect with Planck and BOSS data,” *Phys. Rev.* **D97** no. 2, (2018) 023514, [arXiv:1710.10876 \[astro-ph.CO\]](https://arxiv.org/abs/1710.10876).

[61] J. C. Hill, S. Ferraro, N. Battaglia, J. Liu, and D. N. Spergel, “Kinematic Sunyaev-Zel’dovich Effect with Projected Fields: A Novel Probe of the Baryon Distribution with Planck, WMAP, and WISE Data,” *Phys. Rev. Lett.* **117** no. 5, (2016) 051301, [arXiv:1603.01608 \[astro-ph.CO\]](https://arxiv.org/abs/1603.01608).

[62] **Planck** Collaboration, “Planck intermediate results. LIII. Detection of velocity dispersion from the kinetic Sunyaev-Zeldovich effect,” *Astron. Astrophys.* **617** (2018) A48, [arXiv:1707.00132 \[astro-ph.CO\]](https://arxiv.org/abs/1707.00132).

[63] A. Hall and A. Challinor, “Detecting the polarization induced by scattering of the microwave background quadrupole in galaxy clusters,” *Physical Review D* **90** no. 6, (Sep, 2014) 063518, [1407.5135](https://arxiv.org/abs/1407.5135).

[64] N. Battaglia, “The Tau of Galaxy Clusters,” *JCAP* **1608** no. 08, (2016) 058, [arXiv:1607.02442 \[astro-ph.CO\]](https://arxiv.org/abs/1607.02442).

[65] C. M. Hirata, “Tidal alignments as a contaminant of redshift space distortions,” *Mon. Not. Roy. Astron. Soc.* **399** (2009) 1074, [arXiv:0903.4929 \[astro-ph.CO\]](https://arxiv.org/abs/0903.4929).

[66] M. S. Madhavacheril, N. Battaglia, K. M. Smith, and J. L. Sievers, “Cosmology with kSZ: breaking the optical depth degeneracy with Fast Radio Bursts,” [arXiv:1901.02418 \[astro-ph.CO\]](https://arxiv.org/abs/1901.02418).

[67] M. Schmittfull and U. Seljak, “Parameter constraints from cross-correlation of CMB lensing with galaxy clustering,” *Phys. Rev.* **D97** no. 12, (2018) 123540, [arXiv:1710.09465 \[astro-ph.CO\]](https://arxiv.org/abs/1710.09465).

[68] D. H. Weinberg, R. Dave, N. Katz, and L. Hernquist, “Galaxy clustering and galaxy bias in a lambda-CDM universe,” *Astrophys. J.* **601** (2004) 1–21, [arXiv:astro-ph/0212356 \[astro-ph\]](https://arxiv.org/abs/astro-ph/0212356).

[69] A. Gabasch *et al.*, “The evolution of the luminosity functions in the FORS Deep Field from low to high redshift: II. The red bands,” *Astron. Astrophys.* **448** (2006) 101, [arXiv:astro-ph/0510339 \[astro-ph\]](https://arxiv.org/abs/astro-ph/0510339).

Appendix A: Number counts transfer functions

Corrections to relativistic perturbations arise when considering how to map from the observed $(N(z) - \bar{N}(z)) / \bar{N}(z)$ (or the unperturbed $N(z)$) to the theoretical $(N(\bar{z}) - \bar{N}(\bar{z})) / \bar{N}(\bar{z})$. Here we describe the standard linear theory equations used to compute the perturbations in number counts, and the adjustments we make to these equations in order to account for non-Gaussianities and alignment bias.

We define all number counts transfer functions used below. These transfer functions are the same as can be found in literature [10, 11, 45, 47], with two amendments: two additional bias functions are included, one

for alignment bias, b_A [65], and one for primordial non-Gaussianities, b_{NG} [13].

$$\Delta_{\ell}^{\text{D},i}(k) = \int d\chi \tilde{W}_i(\chi) (b_G - b_A/3 + b_{\text{NG}}) S_{\delta_M, \text{syn}}(k, \chi) j_{\ell}(k\chi) \quad (\text{A1})$$

$$\Delta_{\ell}^{\text{RSD},i}(k) = \int d\chi \tilde{W}_i(\chi) (1 + b_A/f) \frac{k^2 S_v(k, \chi)}{aH} j_{\ell}''(k\chi) \quad (\text{A2})$$

$$\Delta_{\ell}^{\text{lens},i}(k) = \ell(\ell+1) \int d\chi \tilde{W}_i(\chi) \int_0^{\chi} d\chi' \frac{2 - 5s(\chi')}{2} \frac{\chi - \chi'}{\chi\chi'} S_{\phi+\psi}(k, \chi') j_{\ell}(k\chi') \quad (\text{A3})$$

$$\Delta_{\ell}^{\text{D}1,i}(k) = \int d\chi \tilde{W}_i(\chi) \left(\frac{\mathcal{H}'}{\mathcal{H}^2} + \frac{2 - 5s}{\chi\mathcal{H}} + 5s - f_{\text{evo}} \right) k S_v(k, \chi) j_{\ell}'(k\chi) \quad (\text{A4})$$

$$\Delta_{\ell}^{\text{D}2,i}(k) = \int d\chi \tilde{W}_i(\chi) (f_{\text{evo}} - 3) \mathcal{H} S_v(k, \chi) j_{\ell}(k\chi) \quad (\text{A5})$$

$$\Delta_{\ell}^{\text{P}1,i}(k) = \int d\chi \tilde{W}_i(\chi) \left(\frac{\mathcal{H}'}{\mathcal{H}^2} + \frac{2 - 5s}{\chi\mathcal{H}} + 5s - f_{\text{evo}} + 1 \right) S_{\psi}(k, \chi) j_{\ell}(k\chi) \quad (\text{A6})$$

$$\Delta_{\ell}^{\text{P}2,i}(k) = \int d\chi \tilde{W}_i(\chi) (-2 + 5s) S_{\phi}(k, \chi) j_{\ell}(k\chi) \quad (\text{A7})$$

$$\Delta_{\ell}^{\text{P}3,i}(k) = \int d\chi \tilde{W}_i(\chi) \frac{1}{\mathcal{H}} S_{\phi'}(k, \chi) j_{\ell}(k\chi) \quad (\text{A8})$$

$$\Delta_{\ell}^{\text{P}4,i}(k) = \int d\chi \tilde{W}_i(\chi) \left(\frac{\mathcal{H}'}{\mathcal{H}^2} + \frac{2 - 5s}{\chi\mathcal{H}} + 5s - f_{\text{evo}} \right) \int_0^{\chi} d\chi' S_{(\phi+\psi)'}(k, \chi') j_{\ell}(k\chi') \quad (\text{A9})$$

$$\Delta_{\ell}^{\text{P}5,i}(k) = \int d\chi \tilde{W}_i(\chi) \frac{1}{\chi} \int_0^{\chi} d\chi' (2 - 5s(\chi')) S_{\phi+\psi}(k, \chi') j_{\ell}(k\chi') , \quad (\text{A10})$$

where χ is comoving distance and the redshift-space window function

$$W_i(z) \equiv \left| \frac{d\chi}{dz} \right| \tilde{W}_i(\chi) \quad (\text{A11})$$

is a tophat function in redshift, i.e., nonzero and constant in the i -th redshift bin, and is normalized so that its integral over redshift is unity. The transfer functions for determining various fields from primordial perturbations are noted by $S_{\delta_M, \text{syn}}$ for the synchronous gauge matter density, S_{ϕ} and S_{ψ} for the Newtonian potentials, and S_v for the scalar velocity field as defined in [27], which is related to the divergence of the velocity field θ as $S_{\theta} = k^2 S_v$. The bias due to non-Gaussianities (NG) is described by

$$b_{\text{NG}}(k, z) = 3f_{\text{NL}}(b_G(k, z) - 1) \Omega_m H_0^2 \delta_c / (k^2 T(k) S_{\psi}) , \quad (\text{A12})$$

with $\delta_c = 1.686$ the linearized collapse threshold.

The remaining bias functions introduced in Eqs. (A1)–(A10) are defined with respect to the *background* source population. Specifically we can take Eq. (A1) as the definition of the galaxy bias (b_G), and use the parameterization (for a full galaxy sample) based on the simulations of [68] and quoted in the LSST science book [1], of $b_G = 0.95/D(z) \simeq 0.95 + 0.67z$. The magnification bias (s) and evolution bias (f_{evo}) are defined as

$$s(\chi) \equiv \frac{5}{2} \frac{n_s(\chi, \ln L_{\text{cut}})}{\mathcal{N}(\chi, > \ln L_{\text{cut}})} , \quad (\text{A13})$$

$$f_{\text{evo}}(\chi) \equiv \frac{\partial \ln a^3 \mathcal{N}(\chi, > \ln L_{\text{cut}})}{\partial \ln a} . \quad (\text{A14})$$

Here, the quantity n_s is the luminosity function: the galaxy number counts density per luminosity on a spatial hypersurface, ie. not projected onto a lightcone,

$$n_s \equiv \frac{\# \text{ galaxies}}{dV d\ln L} , \quad (\text{A15})$$

and \mathcal{N} is the integrated number density above a threshold luminosity, derived from the luminosity function,

$$\mathcal{N}(\chi, > \ln L_{\text{cut}}) \equiv \int_{\ln L_{\text{cut}}}^{\infty} d\ln L' n_s(\chi, \ln L') . \quad (\text{A16})$$

We model the evolution and magnification biases following the approach outlined in Appendix B.4 of [45]. Explicitly, we assume a Schechter luminosity function of the form

$$n_s(M)dM = 0.4 \ln(10) \phi_* \left[10^{0.4(M_* - M)} \right]^{\alpha+1} \exp \left[-10^{0.4(M_* - M)} \right] dM. \quad (\text{A17})$$

To model the full sample of galaxies we use the r' -band luminosity function found by [69] to approximate the r band luminosity function,

$$M_*(z) = M_0 + g \ln(1 + z), \quad (\text{A18})$$

$$\phi_*(z) = (\phi_0 + \phi_1 z + \phi_2 z^2) [10^{-3} \text{ Mpc}^{-3}]. \quad (\text{A19})$$

The parameters of this model have the explicit values: $\alpha = -1.33$, $g = -1.25$, $M_0 = -21.49$, $\phi_0 = 2.59$, $\phi_1 = -0.136$, and $\phi_2 = -0.081$.

We then relate the absolute magnitude in Eq. (A17) to an apparent magnitude, m , via

$$M = m - 25 - 5 \log_{10} \left[\frac{d_L(z)}{1 \text{ Mpc} h^{-1}} \right] + \log_{10} h - k(z), \quad (\text{A20})$$

where the d_L is the luminosity distance and k is a k -correction due to the corresponding galaxy's spectral energy distribution redshifted to z . We use the extrapolated values of $k(z)$ found in [45] (with $k(z) \propto z$). The quantities, s and f_{evo} (and their redshift dependence) will thus depend on the magnitude limit of the survey in question (we need to integrate Eq. (A16) to M_{cut}). Here we use the limit $m_{\text{cut}} = r = 25.3$ as a representative choice for an LSST type survey [1], although we also explore $m_{\text{cut}} = r = 26.3, 27.3$.

Lastly, and explicitly, we consider the general relativistic terms to include

$$\Delta_{\ell}^{\text{N,GR},i} = \Delta_{\ell}^{\text{D1},i} + \Delta_{\ell}^{\text{D2},i} + \Delta_{\ell}^{\text{P1},i} + \Delta_{\ell}^{\text{P2},i} + \Delta_{\ell}^{\text{P3},i} + \Delta_{\ell}^{\text{P4},i} + \Delta_{\ell}^{\text{P5},i}. \quad (\text{A21})$$

The remaining lensing, RSD, and intrinsic perturbation terms we do not consider as part of the relativistic effects. Together, both the relativistic and non-relativistic contributions comprise the first-order gauge-independent observable angular power spectrum.

Appendix B: Remote dipole (kSZ) transfer functions

The contributions to the remote dipole field transfer function are given as

$$\Delta_{\ell}^{A,i}(k) = \frac{b_v}{2\ell + 1} \int d\chi W_i(\chi) [\ell j_{\ell-1}(k\chi) - (\ell + 1) j_{\ell+1}(k\chi)] \mathcal{K}^A(\chi) \quad (\text{B1})$$

where b_v is an overall bias in the amplitude of the reconstructed remote dipole field that arises due to uncertainty in the electron density field, the “optical depth bias”, and the kernels \mathcal{K}^A are given by one of

$$\mathcal{K}^{\text{LD}}(\chi) = -k S_v(k, \chi) \quad (\text{B2})$$

$$\mathcal{K}^{\text{RD}}(\chi) = k S_v(k, \chi_{\text{CMB}}) [j_0(k\Delta\chi) - 2j_2(k\Delta\chi)] \quad (\text{B3})$$

$$\mathcal{K}^{\text{SW}}(\chi) = 3 \left(2S_{\psi}(k, \chi) - \frac{3}{2} \right) j_1(k\Delta\chi) \quad (\text{B4})$$

$$\mathcal{K}^{\text{ISW}}(\chi) = 6 \int_{\chi_{\text{CMB}}}^{\chi} d\chi' \frac{dS_{\psi}(k, \chi')}{d\chi'} j_1(k\Delta\chi') \quad (\text{B5})$$

for the various terms A (local Doppler LD, remote Doppler RD, Sachs-Wolfe SW, and integrated Sachs-Wolfe ISW) that contribute to the remote dipole field, and for $\Delta\chi \equiv \chi - \chi_{\text{CMB}}$. The fiducial optical depth bias value is chosen to be unity, $b_v = 1$, and is marginalized over independently in each redshift bin considered. Explicitly, we consider the general relativistic (or primary CMB) terms to include

$$\Delta_{\ell}^{\text{kSZ,GR},i} = \Delta_{\ell}^{\text{RD},i} + \Delta_{\ell}^{\text{SW},i} + \Delta_{\ell}^{\text{ISW},i}. \quad (\text{B6})$$

The non-relativistic (non-primordial) remaining term is the local Doppler contribution, attributable to only the Newtonian-gauge peculiar velocity of the remote electron. As noted in [27], the Newtonian velocity contribution alone is not a (linear) gauge-invariant quantity, and the observable should include the additional relativistic contributions.